Inorganic Chemistry

Article

pubs.acs.org/IC

Unexpected Electronic Process of H_2 Activation by a New Nickel Borane Complex: Comparison with the Usual Homolytic and Heterolytic Activations

Guixiang Zeng and Shigeyoshi Sakaki*

Fukui Institute for Fundamental Chemistry, Kyoto University, Takano-Nishihiraki-cho 34-4, Sakyo-ku, Kyoto 606-8103, Japan

Supporting Information

ABSTRACT: H−H σ-bond activation promoted by Ni-[MesB(*o*-$Ph_2PC_6H_4)_2$] ($\mathbf{1}^{Mes}$) was theoretically investigated with the density functional theory method. In $\mathbf{1}^{Mes}$, the nickel 3d, 4s, and 4p orbital populations are similar to those of the typical nickel(II) complex. First, one H_2 molecule coordinates with the nickel center to form a dihydrogen complex, **2**, which induces an increase in the nickel 3d and 4p orbital populations and thus a decrease in the nickel oxidation state. Then, the H−H σ-bond is cleaved under the unusual cooperation of the electron-rich nickel center and the electron-deficient borane ligand in a polarized manner, leading to an unprecedented *trans*-nickel(II) hydridoborohydrido complex, **3**. In the transition state, charge transfer (CT) occuring from the H_2 moiety to the $\mathbf{1}^{Mes}$ moiety (0.683 e) is much larger than the reverse CT (0.284 e). As a result, cleavage of the H−H σ-bond affords two positively charged hydrogen atoms. In this process, the boron atomic population and the nickel 4p orbital population increase, but the nickel 3d orbital population decreases. After cleavage of the H−H σ-bond, CT from the nickel 4p orbital to these positively charged hydrogen atoms occurs to afford **3**, where the oxidation state of the nickel center increases to +2. These electronic processes are different from those of the usual homolytic and heterolytic H−H σ-bond activations. Regeneration of $\mathbf{1}^{Mes}$ and the role of the borane ligand in these reactions are also discussed in detail.

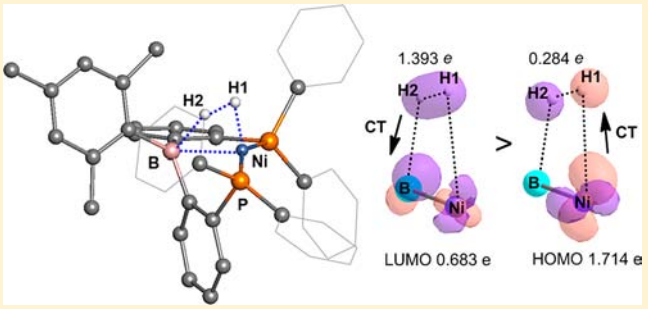

INTRODUCTION

H_2 activation promoted by transition-metal complexes is of great importance in a wide field of chemistry such as hydrogen storage,[1] hydrogenation/reduction catalysis,[2] and bioinorganic chemistry.[3] Usually, the H−H σ-bond is either homolytically or heterolytically cleaved by transition-metal complexes, as displayed in Scheme 1.[4]

Scheme 1. H−H σ-Bond Activation

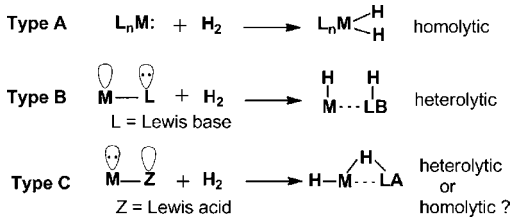

The former cleavage occurs through the oxidative addition of the H−H σ-bond to a metal center to form a dihydride complex (type A in Scheme 1), where the oxidation state of the metal center increases by 2. This kind of reaction is possible for electron-rich late transition metals. The latter reaction generally occurs under the cooperative functions of an electron-deficient transition-metal center and an electron-rich Lewis base (L) ligand, where the metal center and the ligand accept a hydride and a proton, respectively (type B in Scheme 1). In this type of reaction, the oxidation state of the metal center does not change at all. However, the H−H σ-bond cleaved by the cooperation of an electron-rich transition-metal center and an electron-deficient Lewis acid (Z) ligand[5] is rarely reported (type C in Scheme 1).[6] In the M → Z complex, the M center donates two electrons to form a dative bond with the Z-type ligand, where the oxidation state of the M center increases by 2 in a formal sense for this charge-transfer (CT) interaction.[7] In the product, the M−Z bond is broken, but a M−H bond and a M−H−Z bridge are formed, where the oxidation state of the M center is the same as that in the M → Z complex. Seemingly, the oxidation state of the M center does not change in the whole reaction. However, the electronic details of such a kind of reaction have not been elucidated yet. Also, it is not clear in which manner the H−H σ-bond is cleaved in the type C reaction; in other words, is it in a hemolytic, heterolytic, or some other manner?

The borane ligand is one of the well-known Z-type ligands. In transition-metal borane complexes,[8] the transition-metal center is considered as a Lewis base center and the borane ligand is regarded as a Lewis acid ligand. This metal−ligand

Received: August 7, 2012
Published: March 6, 2013

   dx.doi.org/10.1021/ic301733r | Inorg. Chem. 2013, 52, 2844−2853

structure is fit to perform the reaction in the type C activation mode. However, such a kind of complex is seldom employed for H−H σ-bond activation. In 2011, Owen et al. reported a pioneering work in which a rhodium borane complex reacts with two H_2 molecules to produce a dihydridoborohydrido complex at 358.15 K.[5a] However, the mechanistic process of this reaction was not documented in their work.

Another important issue in the chemistry of H_2 activation is to replace noble metals with abundant and cheap metals in the catalysts. In this regard, bioinspired catalysts with such first-row transition metals as iron,[9] nickel,[10] and cobalt[11] have been extensively investigated. Recently, Peters' group synthesized a new nickel borane complex, Ni[MesB(*o*-$Ph_2PC_6H_4)_2$] ($\mathbf{1}^{Mes}$), and found that it facilely reacts with H_2 to produce a *trans*-nickel(II) hydridoborohydrido complex, **3**, at room temperature;[12] see Scheme 2. This is the first report of H−H σ-bond activation promoted by the first-row transition-metal borane complex. As well, the oxidative addition of H_2 to a mononuclear nickel center, leading to a dihydride nickel complex, has not been reported yet. This result suggests that the borane ligand plays an important role in the generation of **3**. Furthermore, $\mathbf{1}^{Mes}$ could be easily recovered through the hydrogenation reaction of styrene catalyzed by **3**. When the mesityl group on the boron atom was replaced by a phenyl group, complex Ni[PhB(*o*-$Ph_2PC_6H_4)_2$](THF) ($\mathbf{1}^{Ph}$**−THF**; THF = tetrahydrofuran) was obtained. Unexpectedly, it could not react with H_2 even at 333.15 K. Peters et al. briefly discussed this phenomenon in their paper and pointed out that the different size of the phenyl group from the mesityl group alter the reactivity of $\mathbf{1}^{Ph}$**−THF**. However, the reason has not been well established.

Scheme 2. H−H σ-Bond Activation by $\mathbf{1}^{Mes}$

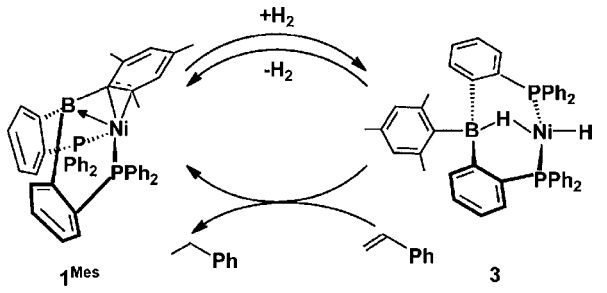

In order to present clear answers to all of these issues mentioned above, we theoretically investigated the reactions shown in Scheme 2. Here, we shed light on (1) the mechanism of H_2 activation mediated by $\mathbf{1}^{Mes}$, (2) the important role of the borane ligand in the reaction, (3) differences in the electronic process between this reaction and the usual homolytic and heterolytic H−H σ-bond activation reactions, and (4) the reason why the nickel borane complex does not react with H_2 when the mesityl group on the boron atom is replaced by a phenyl group.

COMPUTATIONAL DETAILS

All of the geometry optimizations were carried out by the density functional theory (DFT) method[13] with the B3PW91 functional[14] in the gas phase. The effective core potentials of the Stuttgart−Dresden−Bonn group were employed for the core electrons of the nickel center, and the (311111/22111/411/1) basis set was used for its valence electrons.[15] The 6-31++G** basis sets[16] were used for H_2, boron and phosphorus atoms, and the vinyl group of styrene. For other atoms, the 6-31G* basis sets[16a] were used. The vibrational frequency was calculated for each stationary structure to make sure that it is an equilibrium structure or a transition state (TS). The electronic energy in the solution phase (THF) was calculated with the M06 functional.[17] The solvent effect was evaluated by the conductor-like polarizable continuum model (CPCM)[18] with UAKS radii, where the optimized structures in the gas phase were employed. Thermal correction and entropy contributions to the Gibbs energy were taken from the frequency calculations. The reliability of the present computational

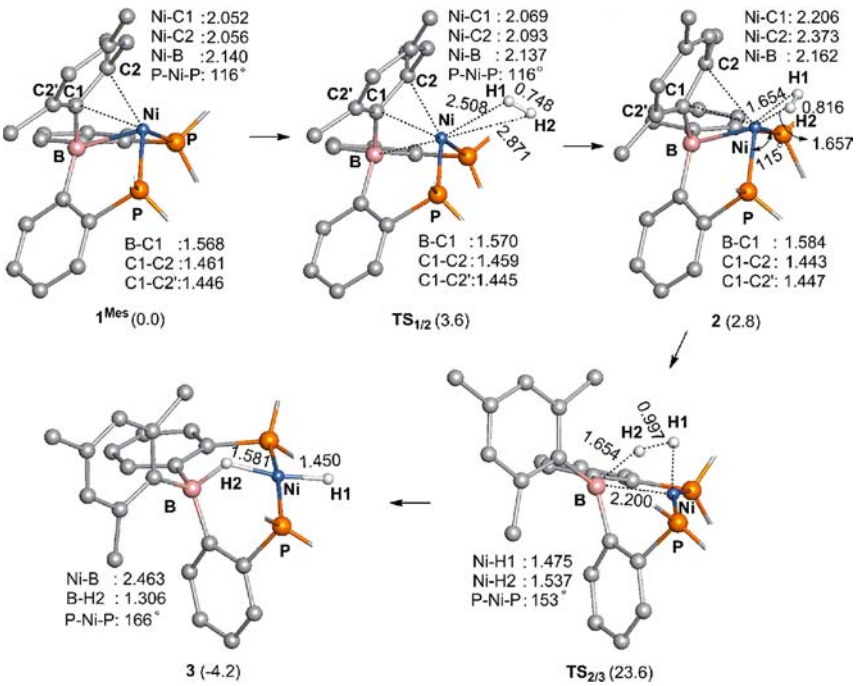

Figure 1. Optimized geometries of all species involved in H−H σ-bond activation promoted by $\mathbf{1}^{Mes}$. Distances are in angstroms. Hydrogen atoms and phenyl groups are omitted for clarity. The relative Gibbs energies are provided next to each species.

dx.doi.org/10.1021/ic301733r | Inorg. Chem. 2013, 52, 2844−2853

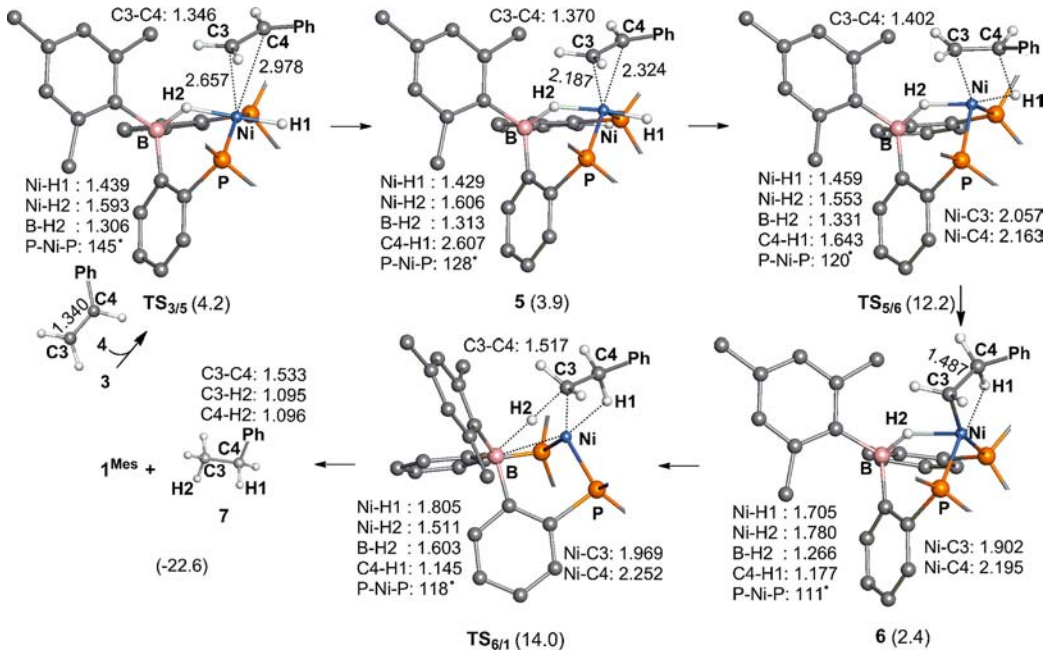

Figure 2. Optimized geometries of all species involved in the hydrogenation reaction of styrene. Distances are in angstroms. Hydrogen atoms and phenyl groups are omitted for clarity. The relative Gibbs energies are provided next to each species.

procedure is briefly discussed on p S3 in the Supporting Information (SI); see Tables S1 and S2. All of these calculations were carried out by the *Gaussian 09* program.[19]

RESULTS AND DISCUSSION

In this section, the discussion is based on the Gibbs energy changes calculated on the singlet potential energy surface, unless otherwise noted. Here, if an intermediate before a TS is less stable than the initial reactant(s) or no intermediate exists before a TS (for example, the first step), the Gibbs activation energy ($\Delta G^{\circ\ddagger}$) is defined as the Gibbs energy difference between the TS and the initial reactant(s). Otherwise, it is the Gibbs energy difference between the TS and the intermediate before the TS. The Gibbs reaction energy (ΔG°) is defined as the Gibbs energy difference between the product and the reactant(s) for a given step.

H−H σ-Bond Activation Mediated by 1^{Mes} and Successive Styrene Hydrogenation: Geometry and Energy Changes. As shown in Figure 1, the boron atom and the mesityl group coordinate with the nickel center in a η^3-coordination mode in $\mathbf{1}^{Mes}$, where Ni−B, Ni−C1, and Ni−C2 distances are 2.140, 2.052, and 2.056 Å, respectively. The C1−C2 bond is moderately elongated to 1.461 Å, which is longer than the C1−C2′ bond (1.446 Å), which does not interact with the nickel center.

First, one H_2 molecule coordinates with the nickel center at the position trans to the boron atom through $\mathbf{TS}_{1/2}$ to afford a dihydrogen complex, **2**. This reaction step occurs with $\Delta G^{\circ\ddagger}$ and ΔG° values of 3.6 and 2.8 kcal/mol, respectively; see Figure 1. When going from $\mathbf{TS}_{1/2}$ to **2**, the Ni−H1 and Ni−H2 distances become shorter from 2.871 and 2.508 Å to 1.654 and 1.657 Å, respectively. Concomitantly, the H1−H2 distance is elongated from 0.748 to 0.816 Å. These features indicate that the interaction between the nickel center and H_2 becomes stronger. This H_2 coordination process also induces other geometrical changes, as follows: (1) The Ni−C1 and Ni−C2 distances are elongated from 2.069 and 2.093 Å in $\mathbf{TS}_{1/2}$ to 2.206 and 2.373 Å in **2**, respectively, suggesting that the mesityl group is gradually moving away from the nickel center as H_2 approaches the nickel center. In **2**, the C1−C2 bond distance (1.443 Å) becomes almost the same as that (1.447 Å) of the C1−C2′ bond, indicating that the C1−C2 bond completely dissociates from the nickel center. (2) The Ni−B bond becomes moderately longer in **2** than in $\mathbf{1}^{Mes}$ by 0.022 Å, suggesting that the Ni → B CT interaction becomes weaker. We will provide the reason why in detail below.

Then, the H1−H2 bond is cleaved through $\mathbf{TS}_{2/3}$ to form a hydridoborohydrido complex, **3**. In $\mathbf{TS}_{2/3}$, the H1−H2 bond distance becomes longer to 0.997 Å. Consistent with this H1−H2 bond elongation, the Ni−H1, Ni−H2, and B−H2 distances become shorter to 1.475, 1.537, and 1.654 Å, respectively. Complex **3** takes a square-planar structure, where the H1 and H2 atoms are at the positions trans to each other with Ni−H1 and Ni−H2 bond distances of 1.450 and 1.581 Å, respectively. Note that the Ni−H2 distance is longer than the Ni−H1 distance. In addition, the B−H2 (1.306 Å) bond distance is longer than the usual B−H bond distance (1.237 Å) of the borohydride compound $[Ph_3BH]^-$.[20] These geometrical features indicate that the H2 atom acts as a bridge to connect the nickel center and the boron atom. In the Ni−H2−B bridge, the B−H2−Ni angle is 117° like that in the typical transition-metal σ-borane complexes.[21] The $\Delta G^{\circ\ddagger}$ and ΔG° values of this reaction step are 23.6 and −7.0 kcal/mol, respectively, indicating that the reaction is thermodynamically favorable. During the reaction, the structure around the nickel center considerably changes from a tetrahedral geometry to almost a planar one, where the P−Ni−P angle significantly increases from 115° to 166°; see Figure 1. At the same time, two five-membered rings formed by the diphosphinoborane ligand and the nickel center in **2** change to two six-membered rings in **3**. These geometrical changes indicate that the ring strain is largely released in this reaction step. To examine the contribution of the release of the ring strain to the reaction, we investigated the reaction of H_2 with a model complex $Ni(PMe_3)_2(BMe_3)$. This

dx.doi.org/10.1021/ic301733r | *Inorg. Chem.* 2013, 52, 2844−2853

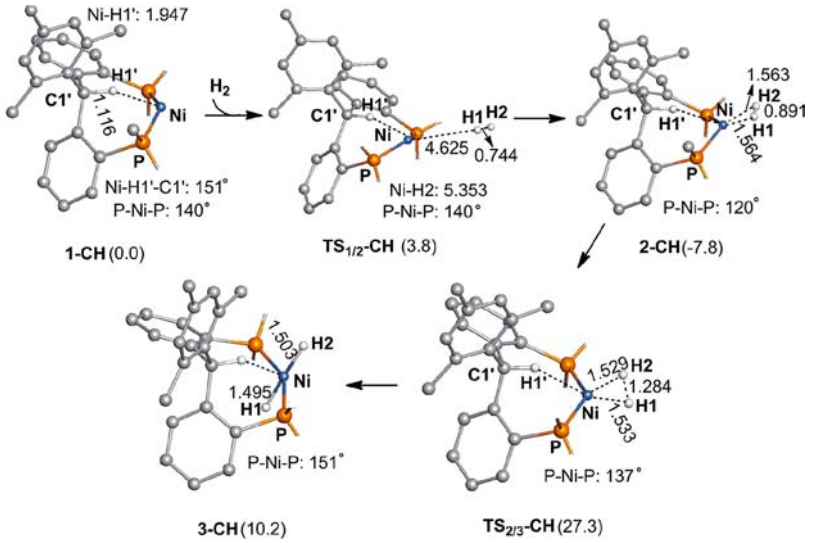

Figure 3. Optimized geometries of all species involved in H−H σ-bond activation promoted by **1**−**CH**. Distances are in angstroms. Hydrogen atoms and phenyl groups are omitted for clarity. The relative Gibbs energies are provided next to each species.

model complex possesses the Ni → B CT interaction but does not contain the ring strain; see Figure S1 in the SI for geometry and energy changes. The model reaction is endothermic by 3.3 kcal/mol. This result indicates that the release of the ring strain plays a crucial role for the exothermicity of the H_2 activation reaction by $\mathbf{1}^{\mathbf{Mes}}$.

We also examined an alternative reaction pathway for the formation of **3**, in which the oxidative addition of the H−H σ-bond to the nickel center occurs first to form a nickel(II) dihydride intermediate and then one hydride migrates from the nickel center to the boron atom to form a Ni−H−B bridge. However, the nickel(II) dihydride intermediate could not be located. The full geometry optimization of such species always leads to the dihydrogen complex **2**, as reported previously,[22] indicating that this alternative reaction pathway can presumably be ruled out here.

Complex **3** further reacts with styrene **4** to regenerate $\mathbf{1}^{\mathbf{Mes}}$. First, the vinyl group of styrene coordinates with the nickel center to form a styrene complex, **5**, through $\mathbf{TS}_{3/5}$, as shown in Figure 2. Upon going from $\mathbf{TS}_{3/5}$ to **5**, the Ni−C3 and Ni−C4 distances considerably decrease from 2.657 and 2.978 Å to 2.187 and 2.324 Å, respectively. Simultaneously, the C3−C4 bond distance becomes longer from 1.346 to 1.370 Å. These geometry changes indicate that the interaction of the vinyl group and the nickel center becomes stronger. Because of such an interaction, the planar geometry around the nickel center changes to a trigonal-bipyramidal one, where the P−Ni−P angle considerably decreases from 166° in **3** to 128° in **5**; see Figure 2. This reaction process also leads to elongation of both the Ni−H2 and B−H2 bond distances by 0.125 and 0.007 Å, respectively, in **5** compared to those in **3**. Elongation of the Ni−H2 distance weakens the trans influence of the hydride H2 ligand, which contributes to the shortening of the Ni−H1 bond from 1.450 Å in **3** to 1.429 Å in **5**. The $\Delta G^{\circ\ddagger}$ and ΔG° values of this step are 8.4 and 8.1 kcal/mol, respectively.

Next, the coordinated vinyl group of the styrene moiety is inserted into the Ni−H1 bond via $\mathbf{TS}_{5/6}$ to produce a monohydride alkyl complex, **6**. From **5** to $\mathbf{TS}_{5/6}$, the vinyl group of the styrene moiety changes from an orientation perpendicular to the Ni−H1 bond to a parallel one. In this process, the C4 atom approaches the H1 atom by 0.964 Å and the Ni−H1 bond becomes longer by 0.03 Å. Also, the Ni−C3 and Ni−C4 distances become shorter by 0.130 and 0.161 Å, respectively, while the C3−C4 bond distance is elongated by 0.032 Å. These geometry changes indicate that the interaction between the nickel center and the vinyl moiety is enhanced. Accordingly, the P−Ni−P angle becomes smaller to 120°, indicating that the geometry around the nickel center becomes further distorted. In **6**, the Ni−C3 and C3−C4 distances are 1.902 and 1.487 Å, respectively, indicating that the Ni−alkyl bond is formed. In addition, the Ni−H1 and C4−H1 distances are 1.705 and 1.177 Å, respectively, and the Ni−H1−C4 angle is 97.5°. These geometrical features indicate that an agostic interaction[23] is formed between the nickel center and the C4−H1 bond. The $\Delta G^{\circ\ddagger}$ and ΔG° values of this insertion step are 12.2 and −1.5 kcal/mol, respectively. Some other interesting geometrical features of **6** are also found. Here, to concentrate on the main topic, we provide such a discussion in the SI, p S7 and Figure S2.

In the last step, $\mathbf{1}^{\mathbf{Mes}}$ is regenerated by the reductive elimination reaction with the release of ethylbenzene (**7**) through $\mathbf{TS}_{6/1}$. From **6** to $\mathbf{TS}_{6/1}$, the B−H2 and Ni−C3 bonds are elongated by 0.337 and 0.067 Å, respectively. On the other hand, the C3−H2 and Ni−H2 distances become shorter to 1.538 and 1.511 Å, respectively. Interestingly, the agostic interaction between the nickel center and the C4−H1 bond is kept in $\mathbf{TS}_{6/1}$, where the Ni−H1 and C4−H1 distances are 1.805 and 1.145 Å, respectively, and the Ni−H1−C4 angle is 97.0°. The $\Delta G^{\circ\ddagger}$ and ΔG° values of this step are 14.0 and −25.0 kcal/mol, respectively, indicating that this process easily occurs.

The influence of the agostic interaction on the hydrogenation reaction of styrene was also examined. By removal of the agostic interaction, **6** and $\mathbf{TS}_{6/1}$ become unstable by 4.8 and 1.4 kcal/mol, respectively. Optimized geometries are provided in Figure S3 in the SI. These calculation results demonstrate that the agostic interaction makes the insertion reaction more thermodynamically favorable and the reductive elimination reaction more kinetically favorable.

Role of the Borane Ligand. In order to explore what role the borane ligand plays in the reactions discussed above, we construct an assumed complex Ni[Mes(CH)(*o*-$Ph_2PC_6H_4)_2$]

dx.doi.org/10.1021/ic301733r | *Inorg. Chem.* 2013, 52, 2844−2853

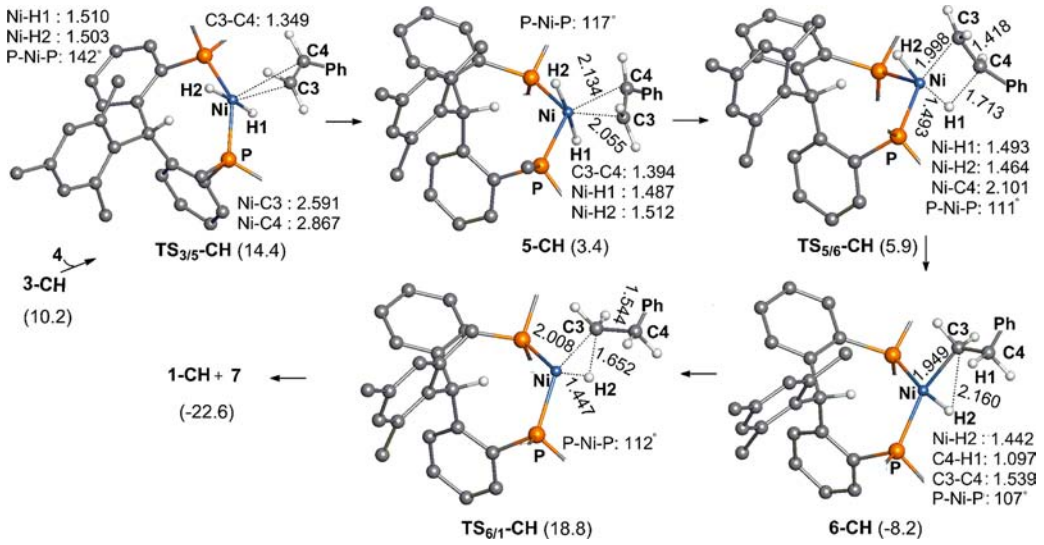

Figure 4. Optimized geometries of all species involved in hydrogenation of styrene mediated by **3**−**CH**. Distances are in angstroms. Hydrogen atoms and phenyl groups are omitted for clarity. The relative Gibbs energies are provided next to each species.

(**1**−**CH**), where the boron atom in $\mathbf{1}^{Mes}$ is substituted for a CH group. In **1**−**CH**, there is no interaction between the nickel center and the C1′ atom as well as the mesityl group, as shown in Figure 3. This is completely different from the η^3-coordination structure of the B−Mes group in $\mathbf{1}^{Mes}$. However, the C1′−H1′ bond forms an attractive interaction with the nickel center, where the C1′−H1′ and Ni−H1′ distances are 1.116 and 1.947 Å, respectively, and the Ni−H1′−C1′ angle is 151.6°. This interaction is an intermediate between the agostic and anagostic interactions.[23]

First, one H_2 molecule coordinates with the nickel center in **1**−**CH**, leading to the formation of a dihydrogen complex, **2**−**CH**, through $\mathbf{TS}_{1/2}$−**CH**. In **2**−**CH**, the Ni−H1, Ni−H2, and H1−H2 distances are 1.564, 1.563, and 0.891 Å, respectively. These Ni−H1 and Ni−H2 distances are shorter than those of **2**, but the H1−H2 bond is longer than that in **2**. These geometrical differences indicate that the interaction between the nickel center and the H_2 moiety is stronger in **2**−**CH** than in **2**. This is consistent with the energetic change that the formation of **2**−**CH** is exothermic by 7.8 kcal/mol but the formation of **2** is endothermic by 2.8 kcal/mol. These results show that the borane ligand is unfavorable for the formation of the dihydrogen complex. This is because the CT occurring from H_2 to the Ni−B moiety leads to a weakening of the Ni → B CT interaction, as discussed above, but no such bond weakening occurs in the reaction of **1**−**CH** with H_2.

Then, the H−H σ-bond is cleaved via $\mathbf{TS}_{2/3}$−**CH** to form a nickel(II) dihydride complex, **3**−**CH**. $\mathbf{TS}_{2/3}$−**CH** takes a tetrahedral structure, which is located in a triplet state.[24] The Ni−H1, Ni−H2, and H1−H2 distances are 1.533, 1.529, and 1.284 Å, respectively. The $\Delta G^{\circ\ddagger}$ and ΔG° values of this step are 35.1 and 18.0 kcal/mol, respectively, which are much larger than those catalyzed by $\mathbf{1}^{Mes}$ (+23.6 and −7.0 kcal/mol, respectively). These differences indicate that the borane ligand facilitates the H−H σ-bond activation and stabilizes the hydridoborohydrido intermediate.

In the following, **1**−**CH** was regenerated via the hydrogenation of styrene **4** mediated by **3**−**CH**. First, the vinyl group of styrene coordinates with the nickel center. As shown in Figure 4, the Ni−C1/Ni−C2 distances in $\mathbf{TS}_{3/5}$−**CH** and **5**−**CH** are 2.591/2.867 and 2.055/2.134 Å, respectively, which are shorter than those in $\mathbf{TS}_{3/5}$ (2.657/2.978 Å) and **5** (2.187/2.324 Å). The C1−C2 bond distance is 1.349 and 1.394 Å in $\mathbf{TS}_{3/5}$−**CH** and **5**−**CH**, respectively, which are longer than those in $\mathbf{TS}_{3/5}$ (1.346 Å) and **5** (1.370 Å). These geometrical differences indicate that the interaction between the nickel center and the vinyl group becomes stronger in the absence of the borane ligand. As a result, a smaller energy barrier is necessary for $\mathbf{TS}_{3/5}$−**CH** (4.2 kcal/mol) than $\mathbf{TS}_{3/5}$ (8.4 kcal/mol). In addition, **5**−**CH** is more stable than **3**−**CH** by 6.8 kcal/mol, whereas **5** is less stable than **3** by 8.1 kcal/mol. These results indicate that the presence of the borane ligand is unfavorable for the coordination of styrene with the nickel center.

Next, the coordinated vinyl group is inserted into the Ni−H1 bond. The Ni−H1 bond distance in **5** (1.429 Å) is shorter than that in **5**−**CH** (1.487 Å), which is consistent with the above discussion that the presence of the borane ligand weakens the trans influence of the hydride H2 ligand. As a result, the insertion reaction becomes easier in the absence of the borane ligand, where the $\Delta G^{\circ\ddagger}$ value of $\mathbf{TS}_{5/6}$−**CH** (5.9 kcal/mol) is smaller than that of $\mathbf{TS}_{5/6}$ (12.2 kcal/mol). Similarly, the absence of the borane ligand is favorable for the insertion product **6**−**CH**. This is because the interaction between the boron atom and the H2 atom destabilizes the alkyl intermediate **6** by forcing it to take a tetrahedral-like geometry. This tetrahedral-like structure is unfavorable for a low-spin d^8 nickel(II) complex bearing a strong alkyl ligand; remember that the low-spin d^8 nickel(II) complex tends to take a square-planar structure when it has such a strong ligand as alkyl. This understanding is consistent with the calculation result that the ΔG° value (−11.6 kcal/mol) of the **6**−**CH** formation reaction is much more negative than that (−1.5 kcal/mol) of **6**.

In the reductive elimination step, the P−Ni−P angle is 112° in $\mathbf{TS}_{6/1}$−**CH** but 118° in $\mathbf{TS}_{6/1}$. This indicates that the ring strain of the Mes(CH)(*o*-$Ph_2PC_6H_4$)$_2$ ligand is larger in $\mathbf{TS}_{6/1}$−**CH** than in $\mathbf{TS}_{6/1}$. As a result, $\mathbf{TS}_{6/1}$−**CH** lies higher than $\mathbf{TS}_{6/1}$ by 4.8 kcal/mol. To exclude the influence of the ring-strain effect, we investigated the reductive elimination reaction mediated by the nickel diphosphine complex Ni(PPh_3)$_2$. In this reaction, the $\Delta G^{\circ\ddagger}$ value decreases to 2.0 kcal/mol. This is much lower than that of $\mathbf{TS}_{6/1}$, indicating that the borane ligand

dx.doi.org/10.1021/ic301733r | *Inorg. Chem.* 2013, 52, 2844−2853

suppresses the reductive elimination reaction. One reason is that the Ni−H2, B−H2, and Ni−C3 bonds must be broken in $\mathbf{TS}_{6/1}$, but only the Ni−H2 and Ni−C3 bonds are broken in the nickel diphosphine system; see Figures S6 and S7 in the SI.

In summary, the presence of the borane ligand facilitates the H−H σ-bond activation step, but it is unfavorable in the styrene hydrogenation reaction.

Electronic Process of the H−H σ-bond Activation Step. In $\mathbf{1}^{\mathbf{Mes}}$, the 3d, 4s, and 4p orbital populations of the nickel center are similar to those of the typical nickel(II) complex **3** (Table 1), indicating that the nickel oxidation state is +2. From $\mathbf{1}^{\mathbf{Mes}}$ to the dihydrogen complex **2**, there are significant changes in the electron populations of the nickel, boron, H1 and H2 atoms, and the phosphine ligand (o-$Ph_2PC_6H_4)_2$; see Figure 5. On one hand, the electron

Table 1. Frontier Orbital Populations of the Nickel Center in the H−H σ-Bond Activation Reaction by $\mathbf{1}^{\mathbf{Mes}}$

	$\mathbf{1}^{\mathbf{Mes}}$	$\mathbf{TS}_{1/2}$	**2**	$\mathbf{TS}_{2/3}$	**3**
3d	9.25	9.27	9.35	9.32	9.25
4s	0.35	0.34	0.36	0.38	0.47
4p	0.45	0.46	0.90	0.94	0.56

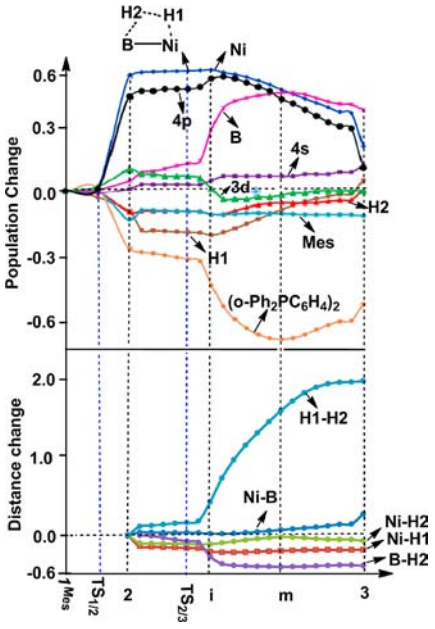

Figure 5. Changes in the bond distance (in Å) and electron populations (in e) along the IRC of H−H σ-bond activation by $\mathbf{1}^{\mathbf{Mes}}$. A positive value represents an increase in the distance and population relative to that in the dihydrogen complex **2** and $\mathbf{1}^{\mathbf{Mes}}$, respectively, and vice versa. Calculations were carried out in the solution phase (THF) with the CPCM model. Mes = 2,4,6-trimethylphenyl.

populations of the H1 and H2 atoms and the phosphine ligand (o-$Ph_2PC_6H_4)_2$ moderately decrease but the nickel and boron atomic populations increase. These results indicate that CT occurs from H_2 to the Ni−B moiety. This CT weakens the Ni−B bond and η^3-coordination of the B−Mes moiety with the nickel center because the lowest unoccupied molecular orbital (LUMO) of **2** contains two antibonding interactions of the nickel d_{z^2} orbital with the boron and C2 p orbitals, respectively; see Scheme 3 for x, y, and z axes. This is the reason why the Ni−B bond is elongated and the mesityl group gradually moves

Scheme 3. LUMO of the Dihydrogen Complex 2

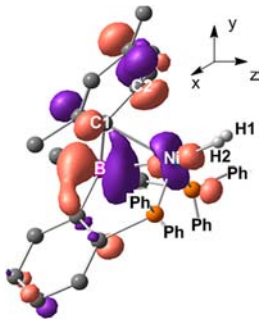

off the nickel center by the coordination of H_2, as discussed above. In this process, the nickel 4p orbital population considerably increases and the 3d and 4s orbital populations moderately increase. These population changes lead to a decrease in the nickel oxidation state.[25]

The electronic process of the H−H σ-bond activation step was explored along the intrinsic reaction coordinate (IRC)[26] calculation. As shown in Figure 5, significant changes of the geometrical parameters and electron populations start to occur around point i, where H−H σ-bond cleavage occurs. Therefore, we discuss the whole reaction process in the following three stages; from **2** to $\mathbf{TS}_{2/3}$, around point i, and after H−H σ-bond cleavage.

Upon going from **2** to $\mathbf{TS}_{2/3}$, the atomic population of the H1 atom further decreases. On the other hand, the nickel 4p orbital population and the boron atomic population further increase, as shown in the upper half of Figure 5. These population changes suggest that CT continues to occur from the H1 atom to the Ni−B moiety. This CT is favorable for H−H σ-bond activation because it decreases the electron population on the σ-bonding molecular orbital (MO) of H_2. In fact, the H−H σ-bond is moderately elongated; see the lower half of Figure 5. In addition, the increase in the boron atomic population suppresses the electron donation from the mesityl (Mes) group to the boron atom, which induces a slight increase in the population of the Mes group.

Around point i (see Figure 5), significantly large changes in the geometry and electron population occur. For example, at point i, the H1 and H2 atomic populations and the nickel 3d orbital population decrease. On the other hand, the boron atomic population and the nickel 4p orbital population increase. These population changes suggest that CT occurs from H_2 to the boron atom and the nickel 4p orbital and reverse CT occurs from the nickel 3d orbital. Simultaneously, the H1−H2 bond is elongated to 1.296 Å and the natural population analysis (NPA) charges of the H1 and H2 atoms are 0.20 and 0.10 e, respectively. These results indicate that the H1−H2 bond is broken and two positively charged hydrogen atoms are formed. We will discuss the reason why in detail below. It is noted that polarization of the H−H σ-bond occurs with CT.

After cleavage of the H−H σ-bond, the H1 and H2 atomic populations start to moderately increase. In contrast, the nickel atomic population, especially the 4p orbital population, starts to decrease, indicating that CT begins to occur from the nickel center to the H1 and H2 atoms. On the other hand, the boron atomic population further increases, whereas the population on the phosphine moiety (o-$Ph_2PC_6H_4)_2$ further decreases. The population of the phosphine moiety reaches the lowest position

dx.doi.org/10.1021/ic301733r | Inorg. Chem. 2013, 52, 2844−2853

at point m. These population changes suggest that CT occurs from the phosphine moiety to the boron atom in the reaction stage between points i and m. In the geometrical aspect, the B−H2, Ni−H2, and Ni−H1 distances change little in this reaction stage, indicating that the Ni−H2−B bridge and the Ni−H1 bond are already formed.

As the reaction proceeds after point m, the H1 and H2 atomic populations keep increasing, whereas the nickel 4p orbital population further decreases until the formation of **3**. Such a feature demonstrates that CT from the nickel center to the H1 and H2 atoms continues to occur. On the other hand, formation of the Ni−H2−B bridge suppresses CT from the phosphine ligand $(o\text{-}Ph_2PC_6H_4)_2$ to the boron atom. As a result, the population of the phosphine ligand $(o\text{-}Ph_2PC_6H_4)_2$ starts to increase. After careful examination, we found that the electron population mainly accumulates on one of the two phenyl groups that are connected with the boron atom; see Table S8 and Figure S8 in the SI. In the geometrical aspect, the H1−H2 distance becomes further longer. This is in accordance with migration of the H1 atom from the position cis to the boron atom toward the trans position, leading to the formation of **3**.

MO Analysis of $TS_{2/3}$. To clarify the reason why H−H σ-bond cleavage leads to the formation of two positively charged hydrogen atoms, we performed MO analysis of $\mathbf{TS}_{2/3}$. Generally, MOs of a total system AB can be represented by a linear combination of MOs of fragments A and B; see eq 1,[28]

$$\varphi_i^{AB} = \sum_m C_{im}^A \varphi_m^A + \sum_n C_{in}^B \phi_n^B \quad (1)$$

where φ_i^{AB} represents the ith MO of complex AB and φ_m^A and φ_n^B are the mth and nth MOs of fragments A and B, respectively. C_{im}^A and C_{in}^B are expansion coefficients of φ_m^A and φ_n^B, respectively. Electron populations of φ_m^A and φ_n^B can be obtained from these coefficients.[29] Here, $\mathbf{TS}_{2/3}$ is divided into such two moieties as H_2 and $\mathbf{1}^{Mes}$. Electron populations of important MOs and MO pictures of the H_2 and $\mathbf{1}^{Mes}$ moieties are shown in Scheme 4. The population on the LUMO of $\mathbf{1}^{Mes}$ considerably increases to 0.683 e, where the LUMO mainly consists of a boron empty p orbital into which the nickel d_{z^2} orbital moderately mixes in an antibonding way; see Scheme 4 for x, y, and z axes. In line with this increase, the population on the σ-bonding MO of H_2 considerably decreases to 1.393 e.

Scheme 4. Important MOs and Their Electron Populations[a] of H_2 and $\mathbf{1}^{Mes}$ in $\mathbf{TS}_{2/3}$

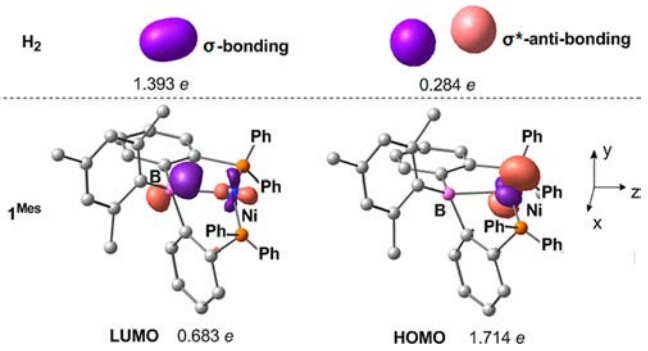

[a]In the unoccupied orbital, the population increases from zero to the number here in the complex. In the doubly occupied orbital, the population decreases from two to the number here in the complex.

These results clearly indicate that CT substantially occurs from the σ-bonding MO of H_2 to the LUMO of $\mathbf{1}^{Mes}$. Furthermore, the population of the σ^*-antibonding MO of H_2 somewhat increases to 0.284 e. Accordingly, the electron population on the highest occupied molecular orbital (HOMO) of $\mathbf{1}^{Mes}$ somewhat decreases to 1.714 e, where the HOMO mainly consists of the nickel $d_{x^2-y^2}$ orbital. These population changes indicate that CT occurs from the doubly occupied nickel $d_{x^2-y^2}$ orbital to the H_2 σ^*-antibonding MO. Both of these CTs contribute to a weakening of the strong H−H σ-bond. However, it is noted that the former CT is much larger than the latter one, indicating that CT from H_2 to $\mathbf{1}^{Mes}$ plays a dominant role in the H−H σ-bond cleavage process. This is consistent with natural bond order analysis along the IRC that H−H σ-bond cleavage leads to the formation of two positively charged hydrogen atoms. When the boron atom is replaced by the CH group, the former CT becomes much weaker, which leads to the formation of two much less negatively charged hydrogen atoms (−0.06 and −0.07 e, respectively). The higher $\Delta G^{\circ\ddagger}$ value of the H_2 activation reaction mediated by **1−CH** also confirms the importance of CT from H_2 to $\mathbf{1}^{Mes}$. These results indicate that the borane ligand facilitates H−H σ-bond cleavage by inducing large CT from H_2 to $\mathbf{1}^{Mes}$.

Comparison with the Usual Homolytic and Heterolytic H−H σ-bond Activations. In order to make a comparison of the present reaction mediated by $\mathbf{1}^{Mes}$ with the usual homolytic and heterolytic H−H σ-bond cleavage reactions (types A and B in Scheme 1, respectively), we investigated the electronic processes of the H_2 activation reactions by $Pt(PMe_3)_2$ and $Pd(H)(OH)(NH_3)$. Note that the H−H σ-bond is cleaved in typical homolytic and heterolytic manners by these two systems, respectively. Optimized geometries are provided in Figure S9 in the SI. In the reaction by $Pt(PMe_3)_2$, oxidative addition of the H−H σ-bond to the platinum center occurs to form a dihydride product. Before the TS, the H1 and H2 atomic populations do not change very much, as shown in Figure 6a. Then, their populations slightly decrease in the stage between TS and point j. At point j, the H−H distance is 1.315 Å,[27] and the NPA charges (0.016 and

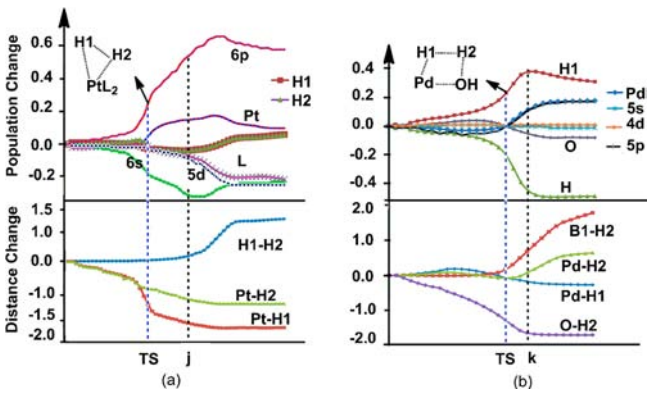

Figure 6. Changes in the bond distance (in Å) and electron populations (in e) along the IRC of the usual homolytic (a)[1] and heterolytic (b) H−H σ-bond activations. A positive value represents an increase in the distance or population relative to that in the initial reactants for homolytic activation and the dihydrogen complex for heterolytic activation and vice versa. L = PMe_3. [1]The Pt−H1 and Pt−H2 bond distances are different here because the IRC calculation stops before reaching the product in which these two bond distances are the same.

dx.doi.org/10.1021/ic301733r | Inorg. Chem. 2013, 52, 2844−2853

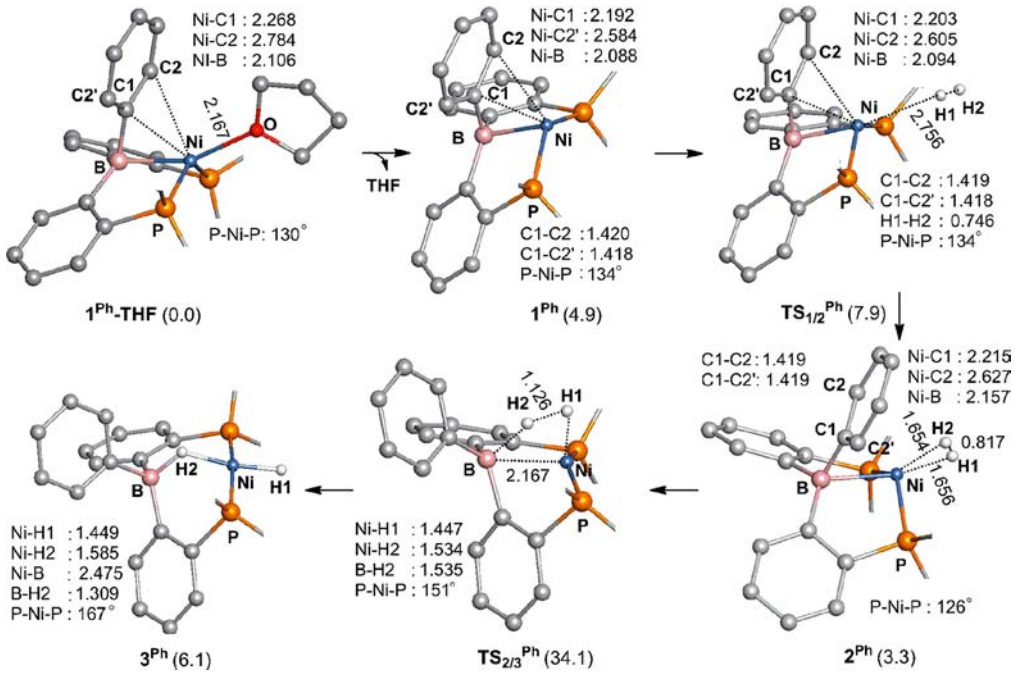

Figure 7. Optimized geometries of all species involved in H−H σ-bond activation promoted by $\mathbf{1}^{Ph}$. Distances are in angstroms. Hydrogen atoms and phenyl groups are omitted for clarity. The relative Gibbs energies calculated at 333.15 K are provided next to each species.

0.012 e, respectively) of H1 and H2 are small with little different from each other, indicating that the H−H σ-bond is homolytically cleaved. After point j, the 5d orbital population of the platinum center gradually decreases, whereas the H1 and H2 atomic populations gradually increase, indicating that CT occurs from the platinum 5d orbital to the H_2 moiety. Accordingly, the oxidation state of the platinum center increases from 0 to +2.

In the reaction by Pd(H)(OH)(NH_3), the H−H σ-bond is cleaved under cooperation of the palladium(II) center (a Lewis acid center) and the OH group (oxygen is a Lewis base center). The H1 atomic population keeps increasing during the reaction, but the H2 atomic population keeps decreasing, as shown in Figure 6b. At point k, the H1−H2 distance is 1.259 Å.[27] The NPA charges of the H1 and H2 atoms are −0.44 and 0.30 e, respectively. These results clearly indicate that the H−H σ-bond is cleaved in a heterolytic manner. The 4d orbital population of the palladium center remains almost constant during the whole reaction process. These features are consistent with our common knowledge that the oxidation state of the palladium(II) center does not change in the heterolytic H−H σ-bond activation process.

As shown in Figures 5 and 6, the population change of the nickel 3d orbital in the H−H σ-bond activation step (from **2** to **3**) is similar to that of the platinum 5d orbital in the homolytic H−H σ-bond activation process but completely different from that of the palladium 4d orbital in the heterolytic activation process. Therefore, it is reasonable to conclude that the oxidation state of the nickel center increases in the H−H σ-bond activation step like that of the platinum center in the oxidative addition reaction. However, the population changes are not perfectly the same between the H_2 activation reactions by $\mathbf{1}^{Mes}$ and Pt(PMe_3)$_2$, as follows: (i) During cleavage of the H−H σ-bond, the nickel 3d orbital population decreases, whereas its 4p and 4s orbital populations moderately increase. In contrast, the platinum 5d orbital population slightly decreases, whereas the platinum 6p orbital population significantly increases and its 6s orbital population significantly decreases. (ii) After cleavage of the H−H σ-bond, the nickel 3d orbital population slightly increases but the 4p orbital population significantly decreases, suggesting that CT mainly occurs from the nickel 4p orbital to the two positively charged hydrogen atoms to form the hydridoborohydrido complex **3**. In contrast, the platinum 5d orbital population significantly decreases after cleavage of the H−H σ-bond, indicating that CT mainly occurs from the platinum 5d orbital to the H_2 moiety to form the dihydride complex **2−Pt**.

In summary, the oxidation state of the nickel center changes during the H_2 activation reaction by $\mathbf{1}^{Mes}$. In $\mathbf{1}^{Mes}$, the oxidation state of the nickel center is +2. It decreases in the dihydrogen complex **2** because the Ni → B CT interaction becomes weaker by the coordination of H_2 with the nickel center. Then, it increases to +2 in the hydridoborohydrido complex **3** because a Ni−H bond and a Ni−H2−B bridge are formed in the H−H σ-bond cleavage step. This process is different from those of the usual homolytic and heterolytic H_2 activation reactions.

Why Does the Reactivity of the Nickel Borane Complex Disappear When the Mesityl Group of the Borane Ligand Is Replaced by a Phenyl Group? As mentioned in the Introduction, if the mesityl group on the boron atom was substituted for a phenyl group, complex $\mathbf{1}^{Ph}$**−THF** was obtained. At room temperature, the dissociation process of the THF ligand is endothermic by 6.1 kcal/mol. We did not find the TS for this dissociation step on the potential energy surface along the Ni−O distance; see Figure S4 in the SI. However, when the bulky mesityl group is introduced, the THF ligand easily dissociates from the nickel center with $\Delta G^{\circ\ddagger}$ and ΔG° values of 0.9 and −8.1 kcal/mol, respectively; see Figure S5 in the SI for optimized geometries. These results agree well with the experimental observations that THF is bound with $\mathbf{1}^{Ph}$ but not with $\mathbf{1}^{Mes}$.

dx.doi.org/10.1021/ic301733r | Inorg. Chem. 2013, 52, 2844−2853

When the temperature goes up to 333.15 K (experimental conditions), the ΔG° value of the THF dissociation reaction from $\mathbf{1}^{\mathbf{Ph}}$**−THF** decreases to 4.9 kcal/mol because the entropy becomes larger at higher temperature. In other words, the generation of a vacant position on the nickel center becomes easier at higher temperature. In the following, one H_2 molecule approaches the nickel center via $\mathbf{TS}_{1/2}{}^{\mathbf{Ph}}$ to form dihydrogen complex $\mathbf{2}^{\mathbf{Ph}}$; see Figure 7 for geometry and energy changes. The $\Delta G^{\circ\ddagger}$ and ΔG° values of this step are 7.9 and 1.2 kcal/mol, respectively. The Gibbs energies calculated at 333.15 K are employed hereafter. Then, the H−H σ-bond is cleaved through a four-center $\mathbf{TS}_{2/3}{}^{\mathbf{Ph}}$, leading to the formation of a *trans*-nickel(II) hydridoborohydrido complex, $\mathbf{3}^{\mathbf{Ph}}$. The $\Delta G^{\circ\ddagger}$ and ΔG° values of this step are 34.1 and 2.8 kcal/mol, respectively. This $\Delta G^{\circ\ddagger}$ values is too high for the reaction to occur at 333.15 K, which is consistent with the experimental results.

The larger $\Delta G^{\circ\ddagger}$ value of the phenyl case comes from two factors. First, the mesityl group is a better electron donor than the phenyl group. As a result, the Ni−B bond in $\mathbf{1}^{\mathbf{Ph}}$ is stronger than that in $\mathbf{1}^{\mathbf{Mes}}$ because CT from the mesityl group to the boron atom is larger than that from the phenyl group. This is consistent with the shorter Ni−B bond distance in $\mathbf{1}^{\mathbf{Ph}}$ (2.088 Å) than in $\mathbf{1}^{\mathbf{Mes}}$ (2.140 Å). Also, the better electron-donating ability of the mesityl group is favorable for stabilizing the borane moiety in the TS; remember that the Ni−B bond is much elongated in the TS. Second, the P−Ni−P moiety relaxes much more in the mesityl case than in the phenyl case, as follows: The P−Ni−P angle increases by 35° upon going from $\mathbf{1}^{\mathbf{Mes}}$ to $\mathbf{TS}_{2/3}$ but by 21° upon going from $\mathbf{1}^{\mathbf{Ph}}$ to $\mathbf{TS}_{2/3}{}^{\mathbf{Ph}}$. To examine the contribution of these two factors, we fixed the Ni−B distance at 2.20 Å (the value in $\mathbf{TS}_{2/3}$) in $\mathbf{1}^{\mathbf{Ph}}$ and $\mathbf{1}^{\mathbf{Mes}}$ and then optimized other geometrical parameters. In this way, we obtained two species without interactions of the phenyl and mesityl groups with the nickel center, which lie higher than $\mathbf{1}^{\mathbf{Ph}}$ and $\mathbf{1}^{\mathbf{Mes}}$ by 26.7 and 1.2 kcal/mol, respectively. This computational result clearly shows that the phenyl system suffers from much larger distortion energy in the TS than the mesityl system, and hence $\mathbf{1}^{\mathbf{Ph}}$ is not reactive for H−H σ-bond activation.

CONCLUSIONS

In this work, we elucidated the reaction mechanism as well as the electronic process of H−H σ-bond activation promoted by a nickel borane complex, $\mathbf{1}^{\mathbf{Mes}}$, with the DFT method. First, a dihydrogen complex, **2**, was formed via the coordination of H_2 to the nickel center. In this step, the Ni−B bond is weakened and the nickel orbital populations significantly increase. These geometrical and population changes lead to a decrease of the nickel oxidation state. Then, the H−H σ-bond is cleaved under the unusual cooperation of the electron-rich nickel center and the electron-deficient borane ligand in a polarized manner, leading to the formation of a *trans*-nickel(II) hydridoborohydrido complex, **3**. The $\Delta G^{\circ\ddagger}$ and ΔG° values of this step are 23.6 and −7.0 kcal/mol, respectively. In $\mathbf{TS}_{2/3}$, CT from the σ-bonding MO of H_2 to the LUMO of the Ni−B moiety (0.683 e) is much larger than that from the occupied $d_{x^2-y^2}$ orbital of the nickel center to the σ^*-antibonding MO of H_2 (0.284 e). As a result, the H−H σ-bond is cleaved into two positively charged hydrogen atoms. Concomitantly, the 3d orbital population of the nickel center decreases. After cleavage of the H−H σ-bond, CT from the nickel center, especially from its 4p orbital, to these positively charged hydrogen atoms starts to occur. It continues until the complete formation of **3**, which leads to an increase of the oxidation state of the nickel center to +2. Such an electronic process is completely different from our common understanding of the usual homolytic and heterolytic H−H σ-bond cleavages.

We also explored the regeneration of $\mathbf{1}^{\mathbf{Mes}}$ through the hydrogenation reaction of styrene promoted by **3**. The hydrogenation reaction occurs through insertion of the vinyl group into the Ni−H1 bond and successive reductive elimination. The insertion reaction produces an alkyl intermediate **6**, which contains an agostic interaction between the nickel center and β-C−H bond. The $\Delta G^{\circ\ddagger}$ and ΔG° values are 12.2 and −1.5 kcal/mol, respectively. In the reductive elimination step, $\mathbf{1}^{\mathbf{Mes}}$ was regenerated with the release of ethylbenzene through $\mathbf{TS}_{6/1}$. In $\mathbf{TS}_{6/1}$, the agostic interaction between the nickel center and β-C−H bond is kept, which is favorable for the stabilization of $\mathbf{TS}_{6/1}$. The $\Delta G^{\circ\ddagger}$ and ΔG° values of this step are 14.0 and −25.0 kcal/mol, respectively.

The role of the borane ligand was clearly discussed. The borane ligand (a) facilitates H−H σ-bond activation through large CT from the H_2 moiety to the Ni−B moiety, (b) stabilizes the intermediate **3** by forming a Ni−H−B bridge, but (3) suppresses regeneration of the catalyst $\mathbf{1}^{\mathbf{Mes}}$ for the presence of the B−H2 bond.

The mesityl group of the borane ligand also plays an important role in the H−H σ-bond activation reaction. In $\mathbf{1}^{\mathbf{Mes}}$, CT from the mesityl group to the boron atom suppresses the Ni → B CT interaction, which weakens the Ni−B bond. In the TS in which the Ni−B σ-bond is elongated, the mesityl group stabilizes the borane moiety. Therefore, substitution of the mesityl group for a worse electron-donating phenyl group suppresses the reaction thermodynamically and kinetically.

ASSOCIATED CONTENT

Supporting Information

Complete representation of ref 19, calculation method of the Gibbs free energy in the solution phase, and M06-calculated electronic energies in THF solvent (E_{ele}), B3PW91-calculated zero-point energy (ZPE), entropies and thermal correction energies (E_{therm}), and Cartesian coordinates of all stationary points located in this work. This material is available free of charge via the Internet at http://pubs.acs.org.

AUTHOR INFORMATION

Corresponding Author

*E-mail: sakaki.shigeyoshi.47e@st.kyoto-u.ac.jp.

Notes

The authors declare no competing financial interest.

ACKNOWLEDGMENTS

This work is financially supported by Grants-in-Aid from the Ministry of Education, Culture, Science, Sport, and Technology through Grants-in-Aid of Specially Promoted Science and Technology (Grant 22000009) and Grand Challenge Project (IMS, Okazaki, Japan). We are also thankful to the computational facility at the Institute of Molecular Science, Okazaki, Japan.

REFERENCES

(1) (a) Hamilton, C. W.; Baker, R. T.; Staubitzc, A.; Manners, I. *Chem. Soc. Rev.* **2009**, *38*, 279 and references cited therein. (b) Grellier, M.; Vendier, L.; Chaudret, B.; Albinati, A.; Rizzato, S.; Mason, S.; Sabo-Etienne, S. *J. Am. Chem. Soc.* **2005**, *127*, 17592. (c) Kaye, S. S.; Long, J. R. *J. Am. Chem. Soc.* **2005**, *127*, 6506.

(d) Durgun, E.; Ciraci, S.; Zhou, W.; Yildirim, T. *Phys. Rev. Lett.* **2006**, *97*, 226102.
(2) (a) Clapham, S. E.; Hadzovic, A.; Morris, R. H. *Coord. Chem. Rev.* **2004**, *248*, 2201 and references cited therein. (b) Tommaso, D. D.; French, S. A.; Catlow, C. R. A. *J. Mol. Struct.: THEOCHEM* **2007**, *812*, 39. (c) Lei, M.; Zhang, W.; Chen, Y.; Tang, Y. *Organometallics* **2010**, *29*, 543. (d) Dub, P. A.; Ikariya, T. *ACS Catal.* **2012**, *2*, 1718.
(3) (a) Wilson, A. D.; Newell, R. H.; McNevin, M. J.; Muckerman, J. T.; DuBois, M. R.; DuBois, D. L. *J. Am. Chem. Soc.* **2006**, *128*, 358. (b) DuBois, M. R.; DuBois, D. L. *Chem. Soc. Rev.* **2009**, *38*, 62 and references cited therein. (c) Bertini, I.; Gray, H. B.; Stiefel, E. I.; Valentine, J. S. *Biological Inorganic Chemistry*, University Science Books: Mill Valley, CA, 1994.
(4) (a) Tye, J. W.; Darensbourg, M. Y.; Hall, M. B. In *Activation of Small Molecules: Organometallic and Bioinorganic Perspectives*; Tolman, W. B., Ed.; Wiley-VCH: Weinheim, Germany, 2006; p 121. (b) Crabtree, R. H. *The Organometallic Chemistry of the Transition Metals*, 5th ed.; John Wiley & Sons: New York, 2005. (c) Jessop, P. G.; Morris, R. H. *Coord. Chem. Rev.* **1992**, *121*, 155. (d) Spessard, G. O.; Miessler, G. L. *Organometallic Chemistry*; Prentice Hall: Upper Saddle River, NJ, 1997. (e) Niu, S.; Hall, M. B. *Chem. Rev.* **2000**, *100*, 353. (f) Torrent, M.; Solà, M.; Frenking, G. *Chem. Rev.* **2000**, *100*, 439.
(5) (a) Green, M. L. H. *J. Organomet. Chem.* **1995**, *500*, 127. (b) King, R. B. *Adv. Chem.* **1967**, *62*, 203. (b) Amgoune, A.; Bourissou, D. *Chem. Commun.* **2011**, *47*, 859.
(6) (a) Tsoureas, N.; Kuo, Y.; Haddow, M. F.; Owen, G. R. *Chem. Commun.* **2011**, *47*, 484. (b) Bonanno, J. B.; Henry, T. P.; Wolczanski, P. T.; Pierpont, A. W.; Cundari, T. R. *Inorg. Chem.* **2007**, *46*, 1222.
(7) Parkin, G. *Organometallics* **2006**, *25*, 4744.
(8) (a) Braunschweig, H.; Colling, M. *Coord. Chem. Rev.* **2001**, *223*, 1. (b) Braunschweig, H.; Dewhurst, R. D. *Dalton Trans.* **2011**, *40*, 549.
(9) (a) Mas-Ballesté, R.; Costas, M.; van den Berg, T.; Que, L., Jr. *Chem.—Eur. J.* **2006**, *12*, 7489. (b) Oldenburg, P. D.; Feng, Y.; Pryjomska-Ray, I.; Ness, D.; Que, L., Jr. *J. Am. Chem. Soc.* **2010**, *132*, 17713. (c) Zhang, P.; Wang, M.; Na, Y.; Li, X.; Jiang, Y.; Sun, L. *Dalton Trans.* **2010**, *39*, 1204. (d) Liu, T.; Chen, S.; O'Hagan, M. J.; DuBois, M. R.; Bullock, R. M.; DuBois, D. L. *J. Am. Chem. Soc.* **2012**, *134*, 6257.
(10) (a) Goff, A. L.; Artero, V.; Jousselme, B.; Tran, P. D.; Guillet, N.; Métayé, R.; Fihri, A.; Palacin, S.; Fontecave, M. *Science* **2009**, *326*, 1384. (b) Hambourger, M.; Moore, T. A. *Science* **2009**, *326*, 1355. (c) Kilgore, U. J.; Roberts, J. A. S.; Pool, D. H.; Appel, A. M.; Stewart, M. P.; DuBois, M. R.; Dougherty, W. G.; Kassel, W. S.; Bullock, R. M.; DuBois, D. L. *J. Am. Chem. Soc.* **2011**, *133*, 5861.
(11) Wiedner, E. S.; Yang, J.; Dougherty, W. G.; Kassel, W. S.; Bullock, R. M.; DuBois, M. R.; DuBois, D. L. *Organometallics* **2010**, *29*, 5390.
(12) Harman, W. H.; Peters, J. C. *J. Am. Chem. Soc.* **2012**, *134*, 5080.
(13) (a) Hohenberg, P.; Kohn, W. *Phys. Rev.* **1964**, *136*, B864. (b) Kohn, W.; Sham, L. J. *Phys. Rev.* **1965**, *140*, A1133.
(14) (a) Becke, A. D. *Phys. Rev. A* **1988**, *38*, 3098. (b) Becke, A. D. *J. Chem. Phys.* **1993**, *98*, 5648. (c) Perdew, J. P. In *Electronic Structure of Solids*, 91th ed.; Ziesche, P., Eschrig, H., Eds.; Akademie Verlag: Berlin, 1991. (d) Burke, K.; Perdew, J. P.; Wang, Y. In *Electronic Density Functional Theory: Recent Progress and New Directions*; Dobson, J. F., Vignale, G., Das, M. P., Eds.; Plenum: New York, 1998.
(15) Dolg, M.; Wedig, U.; Stoll, H.; Preuss, H. *J. Chem. Phys.* **1987**, *86*, 866 and see http://www.tc.uni-koeln.de/cgi-bin/pp.pl?language=en,job=getrefs for a complete reference list.
(16) (a) Rassolov, V. A.; Pople, J. A.; Ratner, M. A.; Windus, T. L. *J. Chem. Phys.* **1998**, *109*, 1223. (b) Clark, T.; Chandrasekhar, J.; Spitznagel, G. W.; Schleyer, P. v. R. *J. Comput. Chem.* **1983**, *4*, 294. (c) Frisch, M. J.; Pople, J. A.; Binkley, J. S. *J. Chem. Phys.* **1984**, *80*, 3265.
(17) Zhao, Y.; Truhlar, D. G. *Theor. Chem. Acc.* **2008**, *120*, 215.
(18) (a) Tomasi, J.; Mennucci, B.; Cammi, R. *Chem. Rev.* **2005**, *105*, 2999. (b) Barone, V.; Cossi, M. *J. Phys. Chem. A* **1998**, *102*, 1995. (c) Cossi, M.; Rega, N.; Scalmani, G.; Barone, V. *J. Comput. Chem.* **2003**, *24*, 669.
(19) Frisch, M. J.; et al. *Gaussian 09*, revision A.01; Gaussian, Inc.: Wallingford, CT, 2009.
(20) In **3**, the boron atom is coordinated with three phenyl groups and a hydride. By removal of the influence of the M−H−B bridge in **3**, we employ $[Ph_3BH]^-$ as a model of a borohydride to evaluate the usual B−H bond distance. $[Ph_3BH]^-$ was fully optimized with the B3PW91 functional in the gas phase. For the boron and hydride atoms, the 6-31++G* basis set was used. For other atoms, the 6-31G* basis set was employed.
(21) (a) Pandey, K. K. *Coord. Chem. Rev.* **2009**, *253*, 37 and references cited therein. (b) Pandey, K. K. *Dalton Trans.* **2012**, *41*, 3278.
(22) Ohnishi, Y.-y.; Nakao, Y.; Sato, H.; Sakaki, S. *J. Phys. Chem. A* **2007**, *111*, 7915.
(23) (a) Brookhart, M.; Green, M. L. H. *J. Organomet. Chem.* **1983**, *250*, 395. (b) Braga, D.; Grepioni, F.; Tedesco, E.; Biradha, K.; Desiraju, G. R. *Organometallics* **1997**, *16*, 1846. (c) Brookhart, M.; Green, M. L. H.; Parkin, G. *Proc. Natl. Acad. Sci. U.S.A.* **2007**, *104*, 6908.
(24) We tried to locate the singlet TS of this step but failed.
(25) Here, it is certain that the oxidation state of the nickel center decreases. However, it is not clear which oxidation state the nickel center takes in **2** because the Ni−B bond is elongated but not completely broken by the coordination of H_2. The sum of the nickel 3d, 4s, and 4p orbital populations in **2** is similar to that of a typical nickel(0) dihydrogen complex, $Ni(PPh_3)_2(H_2)$ (**2−P**); see Table S3 in the SI. One of the plausible understandings is that the nickel center takes a zero oxidation state.
(26) (a) Fukui, K. *Acc. Chem. Res.* **1981**, *14*, 363. (b) Hratchian, H. P.; Schlegel, H. B. In *Theory and Applications of Computational Chemistry: The First 40 Years*; Dykstra, C. E., Frenking, G., Kim, K. S., Scuseria, G., Eds.; Elsevier: Amsterdam, The Netherlands, 2005; pp 195−249.
(27) Here, we choose the point that has the H−H bond distance closest to that of point i in Figure 5.
(28) (a) Baba, H.; Suzuki, S.; Takemura, T. *J. Chem. Phys.* **1969**, *50*, 2078. (b) Kato, S.; Yamabe, S.; Fukui, K. *J. Chem. Phys.* **1974**, *60*, 572. (c) Dapprich, S.; Frenking, G. *J. Phys. Chem.* **1995**, *99*, 9352.
(29) Mulliken-type partitioning of the overlap population between two MOs was employed here. However, the problem of Mulliken population analysis is not found here because the electron population of valence MO is considered; note that the problem of the Mulliken population analysis appears when diffuse basis sets are involved but the valence MO is not diffuse: See the SI, p S20 and Table S9.